

## Resonant multiple Andreev reflections in mesoscopic superconducting junctions

G. Johansson

*Department of Microelectronics and Nanoscience, Chalmers University of Technology and Göteborg University, S-412 96 Göteborg, Sweden*

E. N. Bratus

*Department of Microelectronics and Nanoscience, Chalmers University of Technology and Göteborg University, S-412 96 Göteborg, Sweden*  
*and B. Verkin Institute of Low Temperature Physics and Engineering, 310164 Kharkov, Ukraine*

V. S. Shumeiko and G. Wendin

*Department of Microelectronics and Nanoscience, Chalmers University of Technology and Göteborg University, S-412 96 Göteborg, Sweden*

(Received 2 June 1998; revised manuscript received 23 September 1998)

We investigate the properties of subharmonic gap structure (SGS) in superconducting quantum contacts with normal-electron resonances. We find two distinct features of the SGS in resonant junctions which distinguish them from nonresonant point contacts: (i) The odd-order structures on the current-voltage characteristics of resonant junctions are strongly enhanced and have pronounced peaks, while the even-order structures are suppressed, in the case of a normal electron resonance being close to the Fermi level. (ii) Huge current peaks develop at  $eV = \pm 2E_0$  where  $E_0$  indicates the distance of the resonance to the Fermi level. These properties are determined by the effect of narrowing of the resonance during multiple Andreev reflections and by overlap of electron and hole resonances. [S0163-1829(99)14725-8]

### I. INTRODUCTION

Superconducting quantum point contacts are very interesting structures in which the microscopic mechanisms of the current flow through superconducting junctions can be carefully investigated. Quantum point contacts are particularly useful for investigation of such complex transport processes as multiparticle tunneling and coherent multiple Andreev reflections (MAR). The experimental results recently obtained on atomic-size point contacts<sup>1,2</sup> are in good agreement with the theoretical calculations of the subgap current both in the tunnel and contact regimes.<sup>3-7</sup> Moreover, detailed comparison of the calculated subharmonic gap structure with the measured current-voltage characteristics provides deeper insight into the intrinsic properties of atomic-size junctions (number of transport modes, transmissivity of individual modes, etc.).<sup>8</sup>

More complex transport processes may occur in quantum junctions containing atomic clusters or single molecules, e.g., carbon nanotubes.<sup>9,10</sup> In such junctions, highly resistive interfaces between the molecule and the electrodes provide confinement of normal electrons and cause coherent resonant current transport. Resonant quantum transport has also been demonstrated in “artificial molecule” junctions—small metallic dots<sup>11</sup> and gated two-dimensional (2D) electron gas (2DEG) islands.<sup>12</sup> The theory of dc Josephson transport in resonant junctions,<sup>13-16</sup> and the properties of Andreev quantization in quantum resonant junctions,<sup>17-19</sup> have been given considerable attention. However, the properties of MAR in voltage-biased resonant junctions, and the modification of the subharmonic gap structure (SGS) due to normal electron resonances, is much less investigated. Nevertheless, our pre-

liminary results<sup>20</sup> have shown that SGS drastically differs between resonant and nonresonant junctions; similar results were obtained by different methods in Ref. 21. A great advantage of experiments with quantum junctions is the possibility to control the positions of resonant levels by means of electrostatic gates. Thus it is reasonable and desirable to develop a theory where the current is calculated as a function of both the driving voltage and the resonance energy. Such a detailed theory is not necessary for macroscopic junctions where the current must be averaged over randomly distributed resonant levels;<sup>22,23</sup> however it could be a powerful tool for investigation of intrinsic properties of molecular junctions.

In this paper, we calculate the current in resonant quantum junctions as a function of applied voltage and position of the resonance. We present a detailed study of coherent MAR in the presence of Breit-Wigner resonances in the normal electron tunneling and analyze the resonant  $n$ -particle currents. In order to simplify the description of the interplay between MAR and normal electron resonances, we neglect the effects of electron-electron interaction, which however are often important in practice.<sup>24</sup> Our results therefore provide a limiting case for resonant MAR.

The structure of the paper is the following. In Sec. II we derive equations for the inelastic scattering amplitudes in resonant junctions. In Sec. III we discuss properties of the normal electron resonance in the proximity region between the superconducting electrodes. Results of numerical calculations of the current-voltage characteristic for different positions and widths of the resonance are presented in Sec. IV. Finally, Sec. V is devoted to perturbative analysis of resonant SGS.

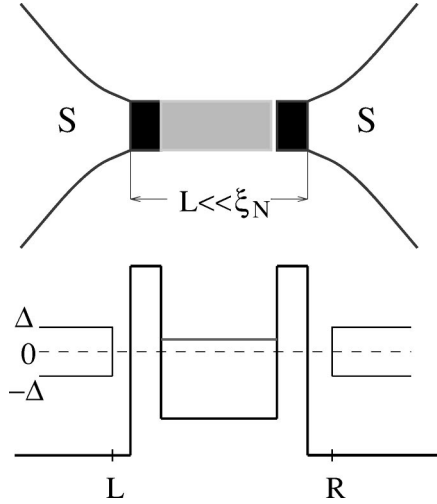


FIG. 1. Schematic picture of the double-barrier junction. Upper part: dark regions are the tunnel barriers; shadowed region is the normal conductor. Lower part: energy diagram showing one normal resonant level inside the superconducting gap. In addition, short normal regions between superconductors and tunnel barriers are introduced for convenience in order to construct the transfer matrix of the junction

## II. SCATTERING AMPLITUDES

We will consider a junction consisting of a ballistic normally conducting region separated from the superconducting electrodes by tunnel barriers, as shown in Fig. 1. The length of the junction  $L$  is assumed to be smaller than the coherence length, and therefore the distance between normal resonances will exceed the superconducting energy gap,  $v_F/L \gg \Delta$  ( $v_F$  is the normal electron Fermi velocity,  $\hbar=1$ ). We will also assume that the resonances are well separated,  $\Gamma \ll v_F/L$ , where  $\Gamma$  is the resonance half-width, and that Coulomb charging effects do not dominate in the subgap voltage region,  $E_C < 2\Delta$ , where  $E_C$  is a Coulomb gap.

We will apply Landauer-Büttiker scattering theory<sup>25-27</sup> extended to superconducting junctions<sup>4</sup> for calculating the current. In voltage-biased superconductive junctions, the quasiparticle scattering is inelastic due to time dependence of the superconducting phase difference across the junction,  $\phi(t) = 2eVt$ , and the scattering state wave functions consist of linear combinations of harmonics (sidebands) with energies  $E_n = E + neV$  shifted by an integer number of quanta  $eV$  with respect to the energy  $E$  of the incoming wave. Below we will consider one single transport mode in the junction and choose the scattering state wave functions in the left (L) and right (R) electrodes have the form

$$\psi_L = e^{-iEt} [\delta_{j1} u_0^+ e^{ik_0^+ x} + \delta_{j2} u_0^- e^{-ik_0^- x}] + \sum_{n=-\infty}^{\infty} e^{-iE_n t} [a_n u_n^- e^{ik_n^- x} + c_n u_n^+ e^{-ik_n^+ x}], \quad (1a)$$

$$\psi_R = e^{i\sigma_z \phi(t)} \left\{ e^{-iEt} [\delta_{j3} u_0^+ e^{-ik_0^+ x} + \delta_{j4} u_0^- e^{ik_0^- x}] + \sum_{n=-\infty}^{\infty} e^{-iE_n t} [b_n u_n^- e^{-ik_n^- x} + f_n u_n^+ e^{ik_n^+ x}] \right\}, \quad (1b)$$

where  $u_n^\pm$  are (non-normalized) two-component elementary solutions of the Bogoliubov-de Gennes equations

$$u_n^\pm = \frac{1}{\sqrt{2}} \begin{pmatrix} e^{\pm \gamma_n/2} \\ \sigma_n e^{\mp \gamma_n/2} \end{pmatrix}. \quad (2)$$

In this equation

$$e^{\gamma_n} = \frac{|E_n| + \xi_n}{\Delta}, \quad \xi_n = \begin{cases} \sqrt{E_n^2 - \Delta^2}, & |E_n| > \Delta, \\ i\sigma_n \sqrt{\Delta^2 - E_n^2}, & |E_n| < \Delta, \end{cases}$$

$$\sigma_n = \text{sgn}(E_n), \quad k_n^\pm = \sqrt{2m(E_F \pm \sigma_n \xi_n)}.$$

Index  $j=1-4$  in Eqs. (1) labels scattering states of the electron- and holelike quasiparticles incoming from the left ( $j=1,2$ ) or right ( $j=3,4$ ). The form of wave functions in Eqs. (1) and (2) assumes that superconducting electrodes serve as equilibrium quasiparticle reservoirs, and that the potential difference between the reservoirs is absorbed into the time-dependent factor  $e^{i\phi(t)}$  in Eq. (1b) due to appropriate choice of the gauge.

To match the wave functions in Eqs. (1) we will apply a transfer-matrix technique. In the present case of an inelastic scattering problem, the connection between  $\psi_L$  and  $\psi_R$  is nonlocal in time, and the corresponding transfer matrix  $\mathbf{T}_{nm}^S$  mixes the sidebands,

$$\begin{pmatrix} A \\ B \end{pmatrix}_{L_n} = \sum_m \mathbf{T}_{nm}^S \begin{pmatrix} A \\ B \end{pmatrix}_{R_m}. \quad (3)$$

The matrix  $\mathbf{T}_{nm}^S$  is a  $4 \times 4$  matrix defined on a space of wave function coefficients,  $A = (A^+, A^-)$ ,  $B = (B^+, B^-)$ ,

$$\psi_n = e^{-iE_n t} [A_n^+ u_n^+ e^{ik_n^+ x} + A_n^- u_n^- e^{-ik_n^- x} + B_n^+ u_n^- e^{ik_n^- x} + B_n^- u_n^+ e^{-ik_n^+ x}]. \quad (4)$$

The transfer matrix in Eq. (3) can be expressed, similarly to the case of unbiased junctions,<sup>19</sup> through a transfer matrix  $T(E)$  associated with elastic electron scattering by the normal junction. Let us introduce auxiliary normal regions between the superconductors and the tunnel barriers of the junction (see Fig. 1); the length of these normal regions is small compared to the coherence length, and will be set equal to zero at the end of the calculations. The wave functions in the normal regions have the form

$$\psi_n^N = \begin{pmatrix} A_n^{N+} e^{ik_n^{N+} x} + A_n^{N-} e^{-ik_n^{N-} x} \\ B_n^{N+} e^{ik_n^{N-} x} + B_n^{N-} e^{-ik_n^{N-} x} \end{pmatrix} e^{-iE_n t}, \quad (5)$$

where  $k_n^{N\pm} = \sqrt{2m(E_F \pm E_n)}$  is the normal electron wave vector. The wave functions Eq. (5) in the left and right normal regions (at points L and R in Fig. 1) are related as

$$\begin{pmatrix} A^N \\ B^N \end{pmatrix}_{L_n} = \mathbf{T}_n^N \begin{pmatrix} A^N \\ B^N \end{pmatrix}_{R_n}, \quad \mathbf{T}_n^N = \begin{pmatrix} T(E_n) & 0 \\ 0 & T(-E_n) \end{pmatrix}. \quad (6)$$

We note that the transfer matrix  $T(E)$  describes scattering of the normal electrons by the actual potential of the junctions at a given voltage, i.e., it includes effects of potential deformation due to applied voltage,  $T(E;V)$ .

Continuous matching at the perfect superconducting–normal-metal (SN) interface at point  $L$  yields in the quasi-classical approximation  $k_n \approx k_n^N \approx k_F$ ,<sup>28</sup>

$$\begin{pmatrix} A^N \\ B^N \end{pmatrix}_{Ln} = \mathbf{T}_n^{NS} \begin{pmatrix} A \\ B \end{pmatrix}_{Ln}, \quad \mathbf{T}_n^{NS} = \begin{pmatrix} e^{\gamma_n/2} & e^{-\gamma_n/2} \\ \sigma_n e^{-\gamma_n/2} & \sigma_n e^{\gamma_n/2} \end{pmatrix}. \quad (7)$$

A matching condition at the right NS interface (point R) is derived in a similar way but an additional time-dependent factor  $e^{i\sigma_z eVt}$  in Eq. (1b) must be taken into account. The latter gives different equations for upper (electron) and lower (hole) components of the coefficient vectors:

$$A_{Rn}^N = \mathbf{P}^+ \mathbf{T}_{n+1}^{NS} \begin{pmatrix} A \\ B \end{pmatrix}_{R(n+1)}, \quad B_{Rn}^N = \mathbf{P}^- \mathbf{T}_{n-1}^{NS} \begin{pmatrix} A \\ B \end{pmatrix}_{R(n-1)}. \quad (8)$$

In this equation,  $\mathbf{P}^\pm$  are projectors on upper/lower vector components.

Combination of Eqs. (6)–(8) gives the following equation for the transfer matrix in Eq. (3):

$$\mathbf{T}_{nm}^S = \sum_{\pm} (\mathbf{T}_n^{NS})^{-1} \mathbf{T}_n^N \mathbf{P}^\pm \mathbf{T}_m^{NS} \delta_{m(n\pm 1)}. \quad (9)$$

The normal electron transfer matrix enters this equation with different arguments  $\pm E_n$ . This energy difference introduces effects of electron-hole dephasing during quasiparticle propagation through the junction. In nonresonant short constrictions, the energy dispersion of the transfer matrix is negligible, and Eq. (9) is equivalent to the matching equation derived in Ref. 4. In resonant junctions (and also in long SNS and SIS junctions<sup>29</sup>) dephasing effects are important.

The matching equations (3) and (9) can be written in an equivalent form,

$$\mathbf{P}^\pm \mathbf{T}_n^{NS} \begin{pmatrix} A \\ B \end{pmatrix}_{Ln} = T(\pm E_n) \mathbf{P}^\pm \mathbf{T}_{Rn\pm 1}^{NS} \begin{pmatrix} A \\ B \end{pmatrix}_{R(n\pm 1)}. \quad (10)$$

Applied to the scattering state wave functions in Eqs. (1), it yields the following recurrences for the scattering amplitudes:

$$\begin{aligned} & e^{\sigma_z \gamma/2} \delta_{n0} \begin{pmatrix} \delta_{j1} \\ \delta_{j2} \end{pmatrix} + e^{-\sigma_z \gamma_n/2} \begin{pmatrix} a \\ c \end{pmatrix}_n \\ &= T(E_n) \left[ e^{\sigma_z \gamma/2} \delta_{(n+1)0} \begin{pmatrix} \delta_{j3} \\ \delta_{j4} \end{pmatrix} + e^{-\sigma_z \gamma_{n+1}/2} \begin{pmatrix} f \\ b \end{pmatrix}_{n+1} \right], \end{aligned} \quad (11a)$$

$$\begin{aligned} & e^{-\sigma_z \gamma/2} \delta_{n0} \begin{pmatrix} \delta_{j1} \\ \delta_{j2} \end{pmatrix} + e^{\sigma_z \gamma_n/2} \begin{pmatrix} a \\ c \end{pmatrix}_n \\ &= T(-E_n) \sigma_n \sigma_{n-1} \left[ e^{-\sigma_z \gamma/2} \delta_{(n-1)0} \begin{pmatrix} \delta_{j3} \\ \delta_{j4} \end{pmatrix} \right. \\ & \quad \left. + e^{\sigma_z \gamma_{n-1}/2} \begin{pmatrix} f \\ b \end{pmatrix}_{n-1} \right]. \end{aligned} \quad (11b)$$

Analytical solutions of the recurrences in Eqs. (11) can be presented in chain-fraction form, (see Appendix A) similar to the case of nonresonant junctions.<sup>3,4</sup>

### III. MODEL FOR RESONANCES

Now we will specify the normal electron transfer matrix  $T(E)$  in the particular case of the double barrier resonant junction shown in Fig. 1. We will restrict ourselves to symmetric junctions,  $T_{11} = T_{22}^* = 1/d(E)$  and  $T_{21} = T_{12}^* = r(E)/d(E)$ . Since the resonances were supposed to be well separated,  $\Gamma, \Delta \ll v_F/L$ , we will consider only one resonance level in the vicinity of the superconducting gap. Assuming a Breit-Wigner resonance form for transmission and reflection amplitudes  $d$  and  $r$  gives

$$d(E) = \frac{i\Gamma}{E - E_r + i\Gamma}, \quad r(E) = -\frac{E - E_r}{E - E_r + i\Gamma}. \quad (12)$$

The position of the resonance level  $E_r$  as well as the resonance half-width  $\Gamma$  are generally dependent on the applied voltage. However, while the subharmonic gap structure is affected in an essential way by the position of the resonance, the dependence on the resonance width is less important. Thus we will assume  $\Gamma = \text{const}$ . We will not specify the voltage dependence of the resonance level position, but rather present the current as a function of two variables: driving voltage and resonance position,  $I(V, E_r)$ . The current voltage characteristics can then be reconstructed from such a dependence by specifying the  $E_r(V)$  dependence determined by the self-consistent distribution of the electric potential across the junction.

The normal electron resonance, being confined between superconducting electrodes, possesses specific properties which will be important for further analysis of the resonant MAR. Since the transfer matrix  $T(E)$  enters the recurrences for the scattering amplitudes in Eq. (11) at two different energies  $\pm E$ , the resonance consists of two, electron and hole, resonances situated symmetrically with respect to the Fermi level,  $E = \pm E_r$  (proximity splitting of the resonance). Within the adopted approach, the current is calculated by using the scattering amplitudes defined in the *superconducting electrodes* [see further Eq. (15)] and the recurrences in Eq. (11) are formulated for these amplitudes. Although equivalent, such an approach is different from the discussion of MAR amplitudes in the normal region of the junction (see, e.g., Ref. 30). Within our approach, the nonsuperconducting region of the junction is considered as a black box and is represented by the transfer matrix  $T(E)$ . Due to the different choices of gauge in the left and right electrodes, the resonance is seen from the left and right electrodes at different energies [cf. Eqs. (7) and (8)]. Indeed, the resonances are seen from the left electrode at  $E = \pm E_r$ , i.e., quasiparticles incoming from the left undergo resonant transition if  $E = \pm E_r$ , while the resonances are seen from the right electrode at  $E = \pm(E_r + eV)$ , as shown in Fig. 2. In the scattering diagram in Fig. 2(c), the resonance therefore is presented with two segments:  $E_n = E_r \leftrightarrow E_{n+1} = E_r + eV$  for the electron resonance, and  $E_n = -E_r \leftrightarrow E_{n-1} = -E_r - eV$  for the hole resonance.

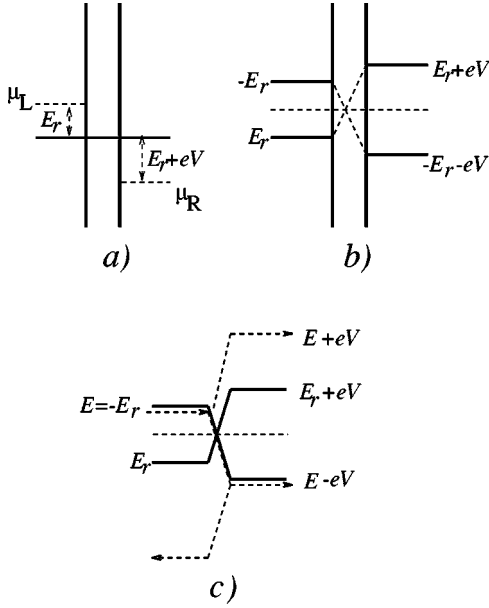


FIG. 2. Energy diagram of resonant junctions under applied voltage. (a) Resonance in the *normal* junction; the distance to the chemical potentials of the left and right electrodes is  $E_r$  and  $E_r + eV$ , respectively. (b) Electron and hole resonances in the *superconducting* junction; the resonance with respect to the global chemical potential is different in the left and right electrodes after equalizing the chemical potentials of the electrodes by means of the gauge transformation. (c) Resonant transition in the scattering diagram.

There is a symmetry between the scattering states originating from the left and right electrodes:

$$\begin{pmatrix} a \\ c \end{pmatrix}_{n,3}(\gamma, \Gamma, E_0) = \sigma_0 \sigma_n \begin{pmatrix} f \\ b \end{pmatrix}_{n,1}(-\gamma, -\Gamma, -E_0), \quad (13)$$

with an analogous relation for the second pair of scattering amplitudes. In Eq. (13),  $E_0 = E_r + eV/2$  is the distance of the normal resonance level with respect to the midpoint between the chemical potentials in the left and right electrodes. Equation (13) leads to a symmetry property of the current which is an even function of the resonance position  $E_0$ :  $I(V, E_0) = I(V, -E_0)$ . Below we will indicate the resonance position by means of the energy  $E_0$  and abbreviate the Breit-Wigner amplitudes (12),

$$d_n^\pm = \frac{i\Gamma}{E_n^\pm + i\Gamma}, \quad r_n^\pm = \frac{E_n^\pm}{E_n^\pm + i\Gamma}, \quad E_n^\pm = E_n \mp (E_0 - eV/2). \quad (14)$$

#### IV. DC CURRENT

In the quasiclassical approximation, the equation for the current reads<sup>3,4</sup>

$$I = \frac{e\Delta}{2\pi} \int_{\Delta}^{\infty} \frac{dE}{\xi} \sum_{n=\text{odd}} \left[ \sum_{j=1,2} (|b_{n,j}|^2 - |f_{n,j}|^2) - \sum_{j=3,4} (|c_{n,j}|^2 - |a_{n,j}|^2) \right] \cosh(\text{Re } \gamma_n) \tanh \frac{E}{2T}. \quad (15)$$

The current in Eq. (15) is calculated using transmitted states (in the right and left electrodes for scattering states  $j=1,2$  and  $j=3,4$  respectively), and it consists of contributions from all odd sidebands. By virtue of the symmetry equations

$$\begin{pmatrix} f \\ b \end{pmatrix}_{n,2}(\gamma, T) = \begin{pmatrix} b \\ f \end{pmatrix}_{n,1}(-\gamma, T^*),$$

$$\begin{pmatrix} a \\ c \end{pmatrix}_{n,2}(\gamma, T) = \begin{pmatrix} c \\ a \end{pmatrix}_{n,1}(-\gamma, T^*), \quad (16)$$

directly following from Eqs. (11) (analogous relations hold for the scattering states  $j=3,4$ ) and the symmetry equations (13), the current in Eq. (15) can be expressed through the sideband contributions

$$K_n = [ |b_n|^2 - |f_n|^2 ] \cosh(\text{Re } \gamma_n) \quad (17)$$

of one single scattering state ( $j=1$ , index  $j$  is omitted),

$$I = \frac{e\Delta}{2\pi} \int_{\Delta}^{\infty} \frac{dE}{\xi} \sum_{n=\text{odd}} [K_n - \bar{K}_n + (E_0 \rightarrow -E_0)] \tanh \frac{E}{2T}, \quad (18)$$

where  $\bar{K}_n = K_n(-\xi_n, -\Gamma)$ .

Equation (18) together with the recurrences in Eqs. (11) provide a basis for numerical calculation of the current. The calculation of scattering amplitudes should obey the boundary condition at  $\pm\infty$  where the amplitudes approach zero. The simplest way to obtain such solutions is to iterate the recurrences from large  $|E_n|$  towards  $E$ . The correct solution will then grow exponentially and numerically “kill” the solution growing at infinity. By this procedure one gets the correct scattering states for each incoming quasiparticle at every energy.

The results of numerical calculation of current-voltage characteristics (IVC) are presented in Fig. 3 for different values of resonance level position  $E_0 = E_r + eV/2 = \text{const}$ . This particular case corresponds to a perfectly symmetric distribution of the electric potential across the junction with  $E_0$  indicating the departure of the resonance level from the Fermi level in equilibrium ( $V=0$ ). The IVC with the resonance level situated at the Fermi level,  $E_0=0$ , shows an onset of the single-particle current at  $eV=2\Delta$  accompanied by a current peak caused by large density of states near the superconducting gap [see below Eqs. (24) and (25)]. Such behavior of the single-particle current has been observed in the experiments on metallic dots<sup>11</sup> and carbon-nanotube junctions.<sup>31</sup> A striking feature of this IVC is the absence of current structure at  $eV=\Delta$ , while the structure at  $eV=2\Delta/3$  is pronounced, consisting of a peak similar to the structure of the single-particle current. Calculation of the IVC at lower voltage, presented in Fig. 4, shows the same feature—only odd subharmonic gap structures are present.

If the resonant level  $E_r$  departs from the Fermi level and  $E_0 = E_r + eV/2 \neq 0$ , the single-particle current onset shifts towards larger voltage,  $eV > 2\Delta$ , and the current peak broadens. A striking feature in this case is the development of a huge current peak at voltages lower than the position of the structure of single-particle current. This peak, associated with resonant pair current (see below Sec. V), appears as soon as  $E_0 > \Delta/2$  and is situated at voltage  $eV = 2E_0$  which

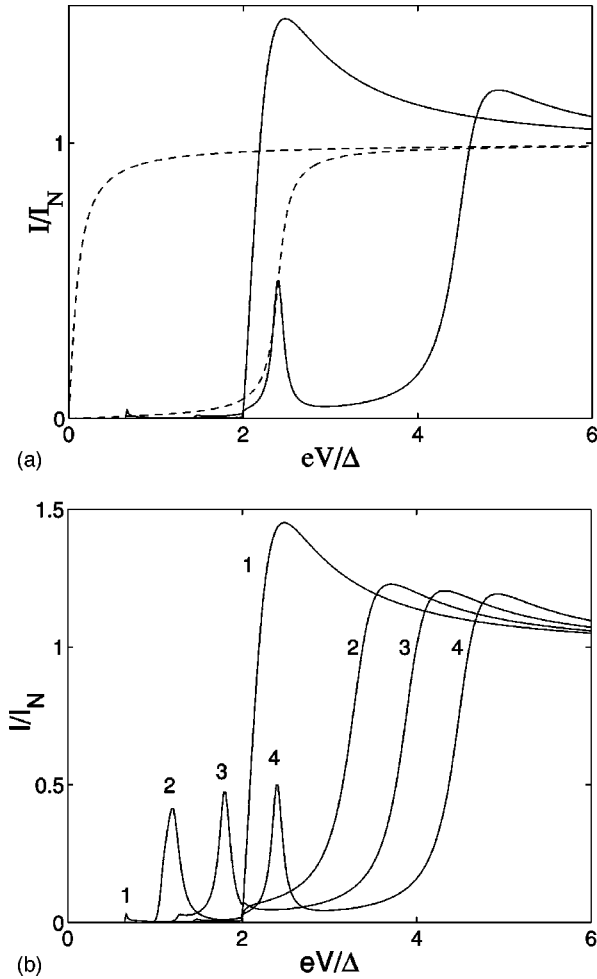


FIG. 3. IVC of symmetric resonant junctions. (a) IVC of normal junction (dashed line) and superconducting junction (solid line),  $E_0/\Delta = 0, 1.2$  (left and right curves, respectively),  $\Gamma/\Delta = 0.05$ . (b) IVC of superconducting junction,  $E_0/\Delta = 0$  (1), 0.6 (2), 0.9 (3), 1.2 (4).

coincides with position of the resonant current onset in normal junctions. If the resonance level departs far from the Fermi level,  $E_0 \gg \Delta$ , the IVC's in the subgap voltage region  $eV < 2\Delta$  approach the form typical for nonresonant point contacts, as could be expected, while strong broadening of the resonance,  $\Gamma \gg \Delta$ , gives rise to SNS-type IVC's, as shown in Fig. 5.

A complete description of the current in resonant junctions is given by the function  $I(V, E_0)$ , as already mentioned in Sec. III. A plot of this function is presented in Fig. 6. The IVCs plotted in Figs. 3–5 correspond to horizontal cuts ( $E_0 = \text{const}$ ) of the plot in Fig. 6. In Fig. 6(a), the light wedgelike region at  $eV > 2\Delta$  corresponds to the resonance single-particle current. The resonant peak of the pair current is seen as the light streaks directed along the lines  $E_0 = \pm eV/2$ , the structure starting at  $eV = \Delta$ . Figure 6(b) presents a similar plot for the region of small voltage,  $eV < \Delta$ . The picture shows quite a complex structure of the current consisting of wedgelike plateaux of the resonant current as well as of light streaks corresponding to current peaks.

In order to interpret the features of the IVC's one needs to analyze the properties of the sideband currents  $K_n$  presented in Eqs. (17) and (A7).

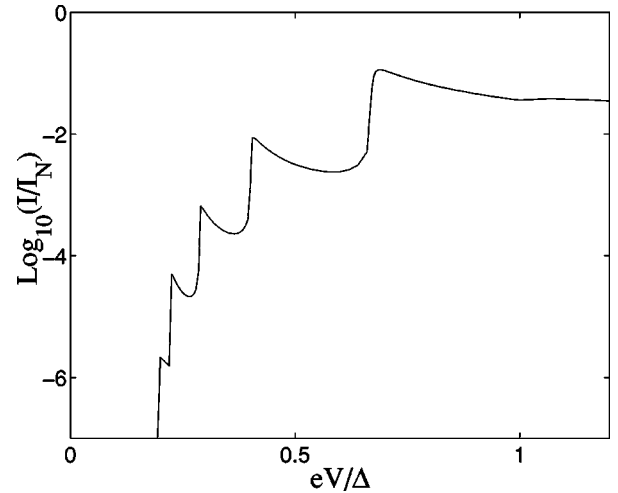


FIG. 4. Subharmonic gap structure on the IVC of a symmetric resonant junction with  $E_0 = 0$ ,  $\Gamma/\Delta = 0.2$ . The structures appear only at  $eV = 2\Delta/n$  with odd  $n$ .

## V. DISCUSSION

A convenient expression for the analysis of the subharmonic gap structure is derived in Appendix B:

$$I_{\text{SGS}}(V, E_0) = \sum_{n=1}^{\infty} I_n(V, E_0),$$

$$I_n(V, E_0) = \frac{e\Delta}{2\pi} \int_{\Delta}^{neV - \Delta} \frac{dE}{\xi} [\tilde{K}_{-n} - \tilde{K}_{-n}^* + (E_0 \rightarrow -E_0)] \tanh \frac{E}{2T}. \quad (19)$$

In Eq. (19) only contributions from processes creating real excitations (transitions across the gap  $E > \Delta \rightarrow E_n < -\Delta$ ) responsible for the subharmonic gap structure<sup>4</sup> are retained, while a contribution of thermal excitations is omitted. Furthermore, the sum over the sideband currents in Eq. (18) is now rearranged in order to explicitly separate the contribu-

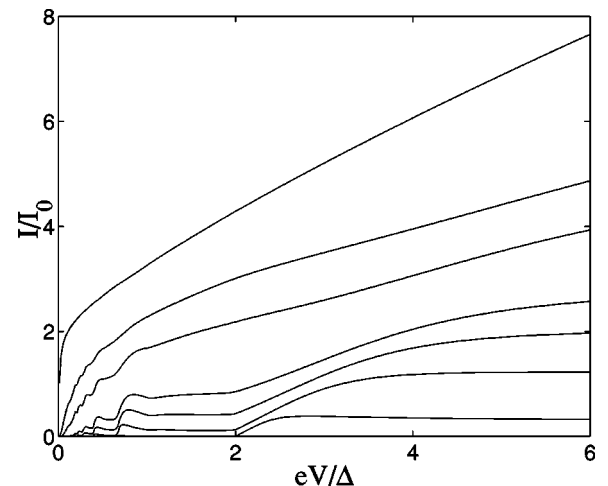


FIG. 5. IVC of symmetric resonant junctions with  $E_0 = 0$  and  $\Gamma/\Delta \in \{0.1, 0.4, 0.7, 1.0, 2.0, 3.0, 10.0\}$  (from bottom to top). The current is normalized by  $I_0 = e\Delta/\hbar\pi$ .

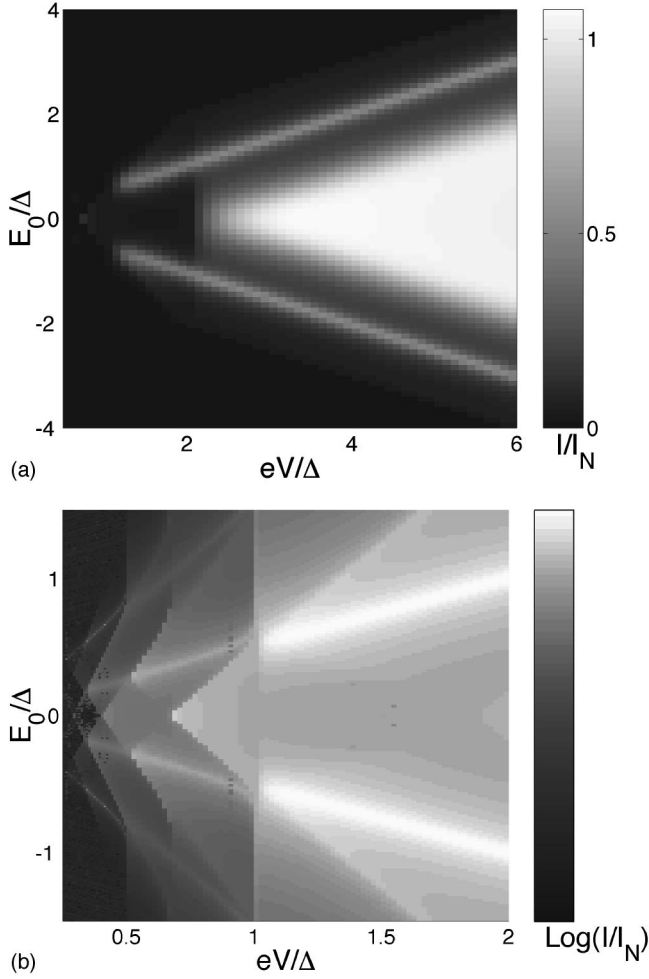


FIG. 6. Intensity plots showing the dependence of the current  $I(V, E_0)$  on the applied bias voltage  $V$  and the resonance position  $E_0$ . (a) Single-particle current and pair current at  $eV > \Delta$  ( $\Gamma = 0.2\Delta$ ). (b) Pair current and high-order currents at  $eV < 2\Delta$  ( $\Gamma = 0.05\Delta$ ).

tions of all inelastic channels [contributions of *even* inelastic channels are hidden in Eq. (18)]. This is done by proper renormalization of the sideband currents  $K_n \rightarrow \tilde{K}_n$  presented in Appendix B, the equation for  $\tilde{K}_n$  being given in Eq. (B9). We will now develop a perturbative analysis of the current in the limit of narrow width of the resonance,  $\Gamma \ll \Delta$ , and zero temperature.

### A. Single-particle current

The single-particle current is given by the first term in Eq. (19). In accordance with Eq. (B9), it has explicit form

$$I_1 = \frac{4e}{\pi} \int_{\Delta}^{eV-\Delta} dE \frac{|E_{-1}| \xi \xi^{-1}}{\Delta^3} \times \left\{ D_0^- \left( \frac{e^{-\gamma}}{P_1} + \frac{e^{\gamma}}{\bar{P}_1} \right) + (E_0 \rightarrow -E_0) \right\}, \quad (20)$$

$P_1$  is defined in Eq. (B10). This current has no contribution from Andreev reflections and it has only one resonance. It is sufficient to consider only scattering states incoming from

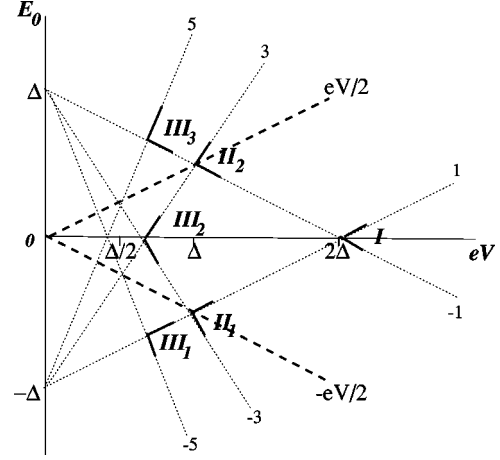


FIG. 7. Resonant regions in the plane  $(eV, E_0)$  for sideband currents  $I_n$ . *I*, *II*, and *III* are resonant regions for single-particle current, pair current and three-particle current, respectively. The resonant regions are bounded by dotted lines  $E_0 = \pm(\Delta - neV/2)$  (labeled with  $\pm n$ ). Bold dashed lines show positions of double resonances.

the left [the first term in curly brackets in Eq. (20)], the resonance equation in this case being  $E_0^- = 2E_0 - eV/2 = 0$  [Eq. (14)]. The resonance is only involved if it belongs to the integration interval. This determines the resonance region  $eV/2 > \Delta + |E_0|$  in the plane  $(V, E_0)$  (region *I* in Fig. 7). The resonant scattering diagram is shown in Fig. 8(a).

In nonresonant junctions, the currents  $\tilde{K}_{-n}$  in Eq. (19) have singularities which are responsible for the main current onset at  $eV = 2\Delta$  and at the subharmonic gap structures at  $eV = 2\Delta/n$ . In resonant junctions, these singularities are washed out due to strong electron-hole dephasing, and the resonant transmissivity is simultaneously renormalized. In the case of the single-particle current in Eq. (20), the onset of nonresonant current is caused by zeros of the function  $P_1$ .

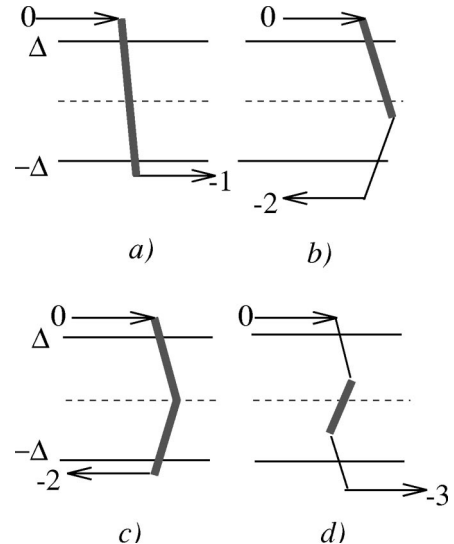


FIG. 8. Resonant scattering diagrams; bold lines show resonant transitions. (a) Resonance in the single-particle current; (b) single resonance in the pair current; (c) double resonance in the pair current; (d) central resonance in the three-particle current.

Calculation of  $P_1$  for the resonant junctions by using the rule in Eq. (B10) and retaining only the resonant scattering amplitude  $d_0^-$  yields

$$\frac{D_0^-}{P_1} \approx \frac{\Delta^4 \Gamma^2}{16 \xi^2 \xi_{-1}^2} \left| E_0^- + \frac{i}{2}(\Gamma_0 + \Gamma_{-1}) \right|^{-2}, \quad (21)$$

where  $\Gamma_n = \Gamma |E_n| / \xi_n$ . Equation (21) shows the transformation of the resonant tunneling probability in the superconducting junctions: the resonance width is broadened due to superconducting density of states  $E/\xi$ . Taking into account Eq. (21) and similar equations for the other terms in Eq. (20), we may present the single-particle current on the form of the Landauer formula,

$$I_1 = \frac{e}{\pi} \int_{\Delta}^{eV-\Delta} dE \tilde{D}_1(E) \quad (22)$$

with the effective single-particle transmission coefficient,

$$\tilde{D}_1(E) = \frac{\Gamma_0 \Gamma_{-1}}{|E_0^- + (i/2)(\Gamma_0 + \Gamma_{-1})|^2}. \quad (23)$$

A similar equation has been derived in Ref. 21 using a different method.

Equations (22) and (23) determine the current in the wedge region in Fig. 6(a). In the limit of  $\Gamma \rightarrow 0$ , the resonant current reads

$$I_1 = \frac{2e^2 \Gamma V_+ V_- \theta[eV - 2(\Delta + |E_0|)]}{V_- \sqrt{(eV_+)^2 - 4\Delta^2} + V_+ \sqrt{(eV_-)^2 - 4\Delta^2}}, \quad (24)$$

where  $eV_{\pm} = eV \pm 2|E_0|$ . This equation quantitatively describes the single-particle current feature in Fig. 3. The current has maximum at the wedge edges and decreases at large  $eV$ , approaching the value for the resonant current in the normal junction  $I_N = e\Gamma$  (see Fig. 3),

$$I_1 = I_N \begin{cases} \frac{2|E_0| + \Delta}{\sqrt{|E_0|(|E_0| + \Delta)}}, & eV = 2(\Delta + |E_0|), \\ 1 + \frac{2\Delta^2}{(eV)^2}, & eV \gg \Delta, E_0. \end{cases} \quad (25)$$

The current peak is the result of enhancement of the effective width of the resonance in Eq. (23) at low energy  $\xi = 0$  ( $E = \Delta$ ). Equation (25) is applicable everywhere except at the wedge vertex,  $E_0 = 0$ ,  $eV = 2\Delta$ , where the current grows without limit. In fact, the current is determined by the singularity, and turns to zero at  $eV = 2\Delta$  due to the shrinking interval of integration in Eq. (22) when the threshold is approached. The maximum current is achieved when the integration interval becomes comparable with the resonance width,  $eV - 2\Delta \sim \Gamma \sqrt{\Delta/(eV - 2\Delta)}$ . These arguments yield estimate for the maximum current at  $eV = 2\Delta$ , namely  $(I_1)_{\max} \sim I_N (\Delta/\Gamma)^{1/3}$

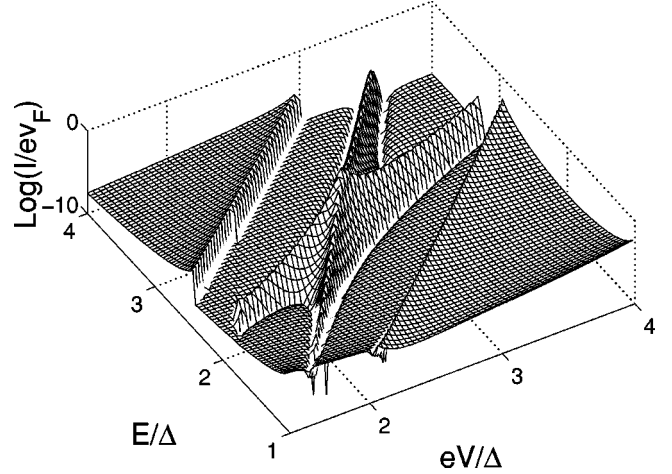


FIG. 9. A 3D plot of the total current density as a function of energy of incoming quasiparticles and bias voltage ( $\Gamma/\Delta = 0.05$ ). The current peak appears at the crossing point of two single resonances.

## B. Pair current

The pair current has the form

$$I_2 = \frac{4e}{\pi} \int_{\Delta}^{2eV-\Delta} dE \frac{|E_{-2}| \xi \xi_{-2}}{\Delta^3} \times \left\{ D_0^- D_{-2}^+ \left( \frac{e^{-\gamma} \varphi_{-2}}{P_2} + \frac{e^{\gamma} \bar{\varphi}_{-2}}{\bar{P}_2} \right) + (E_0 \rightarrow -E_0) \right\}. \quad (26)$$

Restricting again the consideration to quasiparticles incoming from the left, we find that this current gets contributions from two resonances,  $E_0^- = 0$  and  $E_{-2}^+ = 0$ , which simultaneously enter the integration interval within region  $II_1$  in Fig. 7 (region  $II_2$  corresponds to resonant quasiparticles incoming from the right). Therefore, the resonant pair current only appears if the normal resonance is sufficiently far from the Fermi level,  $E_0 > \Delta/2$ , while at  $E_0 < \Delta/2$  the current is nonresonant within the voltage interval  $\Delta < eV < 2\Delta$ . This means in particular that the onset of the pair current at  $eV = \Delta$  is small:  $I_2 \sim I_N (\Gamma/\Delta)^3$  if  $E_0 = 0$ . In regions  $II$ , the pair current undergoes resonant enhancement,  $I_2 \sim I_N (\Gamma/\Delta)^2$  due to independent contributions of two separate resonances [Fig. 8(b)], each contribution being described by the equations similar to Eqs. (22), (23).

The most interesting phenomenon in the resonant pair current is the overlap of the resonances occurring along the lines  $eV = \pm 2|E_0|$  in Fig. 7. The overlap of the resonances produces a huge current peak near these lines, seen as light streaks in the Fig. 6(a) (we note that these lines correspond to the position of the onset of resonant current in normal junctions). The scattering diagram for this case is presented in Fig. 8(c). This crossing of resonances can be clearly seen in the 3D plot of the total current density as a function of energy of incoming quasiparticles and bias voltage in Fig. 9. Applying Eq. (B10) for calculation of  $P_2$  and retaining both the resonant amplitudes  $d_0^-$  and  $d_{-2}^+$ , we obtain

$$\frac{D_0^- D_{-2}^+}{P_2} \approx \frac{\Delta^6 \Gamma^4}{|8\xi\xi_{-1}\xi_{-2}|^2} \left| \left[ E_0^- + i \left( \frac{\Gamma_0 + \Gamma_{-1}}{2} \right) \right] \right. \\ \left. \times \left[ E_{-2}^+ + i \left( \frac{\Gamma_{-1} + \Gamma_{-2}}{2} \right) \right] - \frac{\Gamma^2 \Delta^2}{4|\xi_{-1}|^2} \right|^{-2}. \quad (27)$$

Substituting Eq. (27) into Eq. (26) for the current and collecting the contributions of all scattering modes, we find

$$I_2 = \frac{e}{\pi} \int_{\Delta}^{2eV-\Delta} dE \bar{D}_2(E), \quad (28)$$

where

$$\bar{D}_2(E) = \frac{\Gamma_0 \Gamma_{-2} \Gamma^2 \Delta^2 / 4 |\xi_{-1}|^2}{|\bar{E}_0^- \bar{E}_{-2}^+ - (\Gamma_0 \Gamma_{-2} + \Gamma^2 \Delta^2 / |\xi_{-1}|^2) / 4 + i(\Gamma_{-2} E_0^- + \Gamma_0 E_{-2}^+) / 2|^2}, \quad \bar{E} = E + i\Gamma_{-1}/2. \quad (29)$$

Equation (29) shows a remarkable similarity to the resonant transmissivity of Schrödinger three-barrier structures: the probability to leak outside the superconducting gap through the sidebands  $n=0$  and  $n=-2$  [Fig. 8(c)] corresponding to probability of tunneling through side barriers, while the probability of Andreev reflection by the sideband  $n=-1$  corresponding to transmissivity of a central barrier. Such three-barrier structures have been investigated, e.g., in connection with normal electron transport properties of coupled quantum dots.<sup>32,33</sup> The strong overlap of the resonances is explained by the fact that shift of the resonances is proportional to  $\Gamma^2$  due to Andreev reflection, according to Eq. (29), while the resonance width is proportional to the first power of  $\Gamma$  (the quantity  $\Gamma_{-1}$  is equal to zero at the lines  $eV = \pm 2|E_0|$ ).

In the vicinity of the lines  $eV = \pm 2|E_0|$  and in the limit  $\Gamma \rightarrow 0$ , the pair current has following form:

$$I_2 = I_N \frac{\Gamma^2 eV \sqrt{(eV)^2 - \Delta^2}}{(eV - 2|E_0|)^2 [(eV)^2 - \Delta^2] + \Gamma^2 [2(eV)^2 - \Delta^2]}. \quad (30)$$

(We notice that this formula is valid at all voltages  $eV > \Delta$  because the sideband  $n=-1$  is inside the energy gap if  $eV \approx \pm 2|E_0|$ .) Equation (30) describes the current peak in Fig. 3, the height of the peak

$$(I_2)_{\max} = I_N \frac{2|E_0| \sqrt{4E_0^2 - \Delta^2}}{8E_0^2 - \Delta^2} \quad (31)$$

being comparable to the magnitude of the resonant single-particle current; in particular,  $(I_2)_{\max} = I_N/2$  for  $E_0 \gg \Delta$ .

According to Eq. (30) the resonant pair current tends to zero at large voltage  $eV \gg \Delta, E_0$ , which means that, rigorously speaking, there is no resonant excess current. However, if the resonance is far beyond the gap,  $|E_0| \gg \Delta$ , the current may strongly deviate from the current in the normal junction in the region  $\Delta \ll eV \ll 2|E_0|$  because the single-particle current is nonresonant in this region, while the pair current is resonant. Such an effect is particularly pronounced in junctions where the resonance level follows the chemical potential of one of the electrodes,  $E_0(eV) \pm eV/2 \approx \epsilon = \text{const}$ . The IVC in this case corresponds to cuts in the plot in Fig. 6(a) parallel to the light streaks. In such a case, the peak of the pair current is very broad, and even transforms

into a plateau with a sharp onset at  $eV = \Delta$  ( $\epsilon = 0$ ), as shown in the inset in Fig. 10. The magnitude of the current at the plateau can be found directly from Eq. (A7) when assuming  $E_0 = \epsilon \pm eV/2$  and  $eV = \infty$ ,

$$I_2(\epsilon, \Gamma) = \frac{2e}{\pi} \int_0^\infty dE \cosh(\text{Re } \gamma) \\ \times \frac{2D_0^- \sinh(\text{Re } \gamma) + D_0^- D_0^+ e^{-\text{Re } \gamma}}{|e^\gamma - r_0^- * r_0^+ e^{-\gamma}|^2}, \quad (32)$$

$D_0^\pm = \Gamma^2 / [(E \mp \epsilon)^2 + \Gamma^2]$ . This current as function of  $\epsilon$  is shown in Fig. 10.

There is an interesting difference between the property of the resonance in the single-particle current and that of individual resonances of the pair current. To be specific, let us consider the resonance  $E_0^-$ : in the pair current this resonance

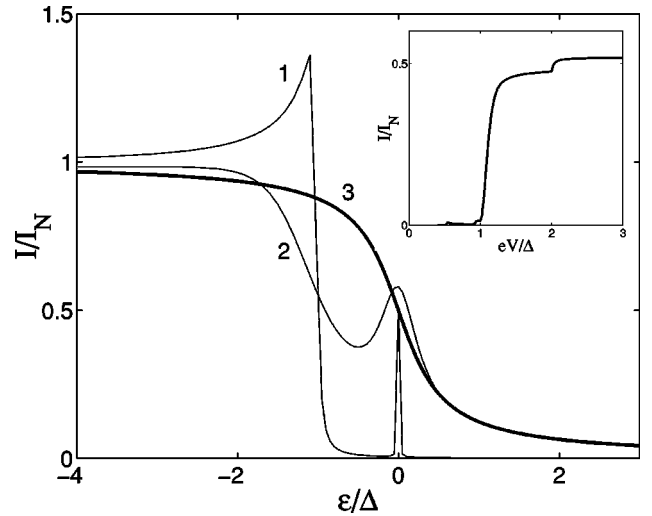


FIG. 10. Current for asymmetric junction at large voltage ( $eV = 1000\Delta$ ) as a function of the position of the resonance  $\epsilon = |E_0| - eV/2$ . The thin lines 1 and 2 denote superconducting junctions with  $\Gamma = 0.01\Delta$  and  $\Gamma = 0.41\Delta$ , respectively; the bold line 3 corresponds to a normal junction with  $\Gamma = 0.41\Delta$ . The difference between currents 2 and 3 shows strong dependence of the excess current on the position of the resonance. Inset shows IVC for  $\epsilon = 0$ : the resonance level coincides with the chemical potential of one of the electrodes.



is more narrow because the quantity  $\Gamma_{-1}$  is imaginary and causes a resonant shift rather than a contribution to the resonance width. The physical reason for this narrowing of the resonance is that direct leakage of a quasiparticle through the sideband  $n = -1$  is blocked, and the only escape from the resonant region into the continuum is through the states of the sideband  $n = 0$ .

### C. High-order currents

The effect of the resonance narrowing is even more important for the third-order current,

$$I_3 = \frac{4e\Delta}{\pi} \int_{\Delta}^{3eV-\Delta} dE \frac{|E_{-3}| \xi \xi_{-3}}{\Delta^3} \left\{ D_0^- D_{-2}^+ D_{-2}^- \times \left( \frac{e^{-\gamma} \varphi_{-3}}{P_3} + \frac{e^{\gamma} \bar{\varphi}_{-3}}{\bar{P}_3} \right) + (E_0 \rightarrow -E_0) \right\}. \quad (33)$$

The third-order current has three resonances at  $E_0^-, E_{-2}^+, E_{-2}^- = 0$  which belong to the interval of integration within the regions  $III_1, III_2, III_3$  in Fig. 7, respectively. The side resonances at  $E_0^-, E_{-2}^- = 0$  are characterized by an effective transmissivity similar to the effective transmissivity of the resonances of the pair current (times an additional factor  $\sim \Gamma^2$ ). The contribution of these resonances to the current is therefore estimated as  $I_3 \sim I_N(\Gamma/\Delta)^4$ . The central resonance  $E_{-2}^+ = 0$  is much more narrow. Indeed, in this case [Fig. 8(d)], direct leakage of the resonant particle into continuum is blocked at both of the sidebands  $n = -1, -2$ , and the particle can escape only through the sideband states  $n = 0, -3$ , traversing the junction one more time. The central resonance determines the current in the vicinity of the threshold  $eV = 2\Delta/3$ ,  $E_0 = 0$ .

Calculation of the quantity  $P_3$  in region  $III_2$  according to Eq. (B10) yields

$$\frac{D_0^- D_{-2}^+ D_{-2}^-}{P_3} \approx \frac{\Delta^4 \bar{\Gamma}_0 \bar{\Gamma}_{-3}}{|4^2 \xi \xi_{-3} E E_{-3}|} \left| \bar{E}_{-2}^+ + \frac{i}{2} (\bar{\Gamma}_0 + \bar{\Gamma}_{-3}) \right|^{-2}, \quad (34)$$

where  $\bar{E}_{-2}^+ = E_{-2}^+ + i(\Gamma_{-1} + \Gamma_{-2})/2 + O(\Gamma^2)$  and  $\bar{\Gamma}_0 = \Gamma_0 D_0^- \Delta^2/4|\xi|^2$ ,  $\bar{\Gamma}_{-3} = \Gamma_{-3} D_{-2}^- \Delta^2/4|\xi_{-2}|^2$ . According to Eq. (34), the resonance width is of the order of  $\bar{\Gamma} \sim \Gamma^3$  which yields giant enhancement of the current,  $I_3 \sim I_N(\Gamma/\Delta)^2$ , exceeding by two orders of  $\Gamma$  the contribution of the side resonances. Such narrowing of the central resonance occurs in the quadrangle region in Fig. 7 bounded by the edges of the resonance region  $III_2$  and regions  $II$ . The current in this region has a form similar to the one in Eq. (22),

$$I_3 = \frac{e}{\pi} \int_{\Delta}^{3eV-\Delta} dE \bar{D}_3(E), \quad (35)$$

with the effective resonant transmissivity

$$\bar{D}_3(E) = \frac{3\bar{\Gamma}_0 \bar{\Gamma}_{-3}}{|\bar{E}_{-2}^+ - i(\bar{\Gamma}_0 + \bar{\Gamma}_{-3})/2|^2}. \quad (36)$$

In the limit of  $\Gamma \rightarrow 0$ , the current becomes

$$I_3 = 6e \bar{\Gamma}_0 \bar{\Gamma}_{-3} / (\bar{\Gamma}_0 + \bar{\Gamma}_{-3})_{E=|E_0|+3eV/2}. \quad (37)$$

The phenomenon of resonance narrowing provides the explanation for the absence of SGS current structure at voltage  $eV = \Delta$ , namely the dominance of the third-order current  $I_3$  at the threshold of the pair current. The current in Eq. (37) is responsible for the light wedgelike region at  $eV < \Delta$  in Fig. 6(b). Similarly to the case of single-particle current, the third-order current in Eq. (37) has a peak at the edges of the wedge with the height increasing proportionally to  $(eV - 2\Delta/3)^{-1/2}$  towards the vertex of the wedge,  $eV = 2\Delta/3$ ,  $E_0 = 0$ . This growth is again limited due to interplay between shrinking integration interval and growing resonance width,  $eV - 2\Delta/3 \sim \Gamma^3 [\Delta/(eV - 2\Delta/3)]^{1/2}$ . This estimate gives a height  $(I_3)_{\max} \sim I_N(\Gamma/\Delta)$  of the current peak at  $eV = 2\Delta/3$ . As one may see in Fig. 6(b), there are no current structures at the edges  $eV = 2(\Delta - |E_0|)$  of the above-mentioned quadrangle where the narrow resonance of three-particle current dies: this is because of the resonant pair current emerges at the same lines, giving rise to a gradual crossover between three-particle current and pair current, both having the magnitude of the order of  $I_N(\Gamma/\Delta)^2$ .

The phenomenon of resonance narrowing results in enhancement of central resonances in all higher odd-order currents, giving rise to current peaks at  $eV = 2\Delta/(2k+1)$ ,  $E_0 = 0$  with heights  $I_{\max} \sim I_N(\Gamma/\Delta)^{2k-1}$ . The magnitude of the current between neighboring peaks is  $I \sim I_N(\Gamma/\Delta)^{2k}$ . Also, the overlap of narrow resonances of even-order currents near the lines  $eV = \pm 2|E_0|$  yields current peaks with heights  $I \sim I_N(\Gamma/\Delta)^{2k}$  within the intervals  $2\Delta/(2k+2) < eV < 2\Delta/(2k+1)$ . These current peaks are clearly seen in Fig. 6(b) in the form of light streaks.

## VI. CONCLUSION

In conclusion, we have considered the effect of normal electron resonant tunneling on the subharmonic gap structure (SGS) in mesoscopic superconducting junctions. In nonresonant tunnel junctions, the SGS consists of sharp onsets and narrow peaks in the current at voltages  $eV = 2\Delta/n$ . In resonant junctions, the SGS is considerably modified depending on the position of the resonance level with respect to the chemical potentials of the electrodes. If the resonance level is situated exactly in the middle between the chemical potentials of electrodes, the odd- $n$  current structures are tremendously enhanced while the even- $n$  current structures are not affected by the resonance. This enhancement is explained by the resonance narrowing during multiple Andreev reflections. When the resonance energy deviates from the midpoint between the chemical potentials of the electrodes, new current structures appear at  $eV = \pm 2E_0$  in the form of current peaks. These features result from overlap of electron and hole resonances.

In our calculations, the Coulomb charging energy was assumed to be smaller than the superconducting gap, and the charging effects were neglected. In experiments on metallic dots<sup>11</sup> and carbon nanotubes,<sup>9,10,31</sup> the opposite situation has been observed with the Coulomb charging energy exceeding the superconducting gap, leading to suppression of the sub-gap current. The charging energy in quantum transport experiments can be reduced by enhancing the capacitance of

the resonant structure, e.g., by using substrates with large dielectric constants. This will allow direct application of our results to such structures. Another way could be to use high- $T_c$  materials with large gap energies for fabrication of superconducting electrodes for the nanotube experiments. Our theory is applicable to ballistic plane junctions with large capacitance such as resonant junctions in high mobility S-2DEG-S devices<sup>34</sup> and atomic plane junctions in layered cuprates (intrinsic Josephson junctions<sup>35</sup>). Current-voltage characteristics of such multimode junctions can be obtained on the basis of our theory by summation of contributions from all transport modes.<sup>20</sup>

### ACKNOWLEDGMENTS

This work was supported by the Swedish Natural Science Research Council (NFR), the Swedish Board for Technical Development (NUTEK), the Swedish Royal Academy of Sciences (KVA), and the New Energy Development Organization (NEDO), Japan.

### APPENDIX A: DERIVATION OF CURRENTS

Following the method of Refs. 3 and 4, we eliminate the Andreev scattering amplitudes  $a_n$  and  $b_n$  from Eqs. (11) for the scattering state  $j=1$  and obtain a closed set of equations for the normal amplitudes  $c_n$  and  $f_n$ ,

$$c_{2n} + V_{2n+1}^- f_{2n+1} + V_{2n-1}^+ f_{2n-1} = \frac{2\xi}{\Delta \Xi_0} \delta_{n0}, \quad (\text{A1})$$

$$f_{2n+1} + V_{2n+2}^+ c_{2n+2} + V_{2n}^- c_{2n} = 0.$$

The coefficients in these equations are

$$V_{2n}^- = d_{2n}^{+*} e^{(\gamma_{2n} + \gamma_{2n+1})/2} / \Xi_{2n+1},$$

$$V_{2n}^+ = -\sigma_{2n} \sigma_{2n-1} d_{2n}^{-*} e^{-(\gamma_{2n} + \gamma_{2n-1})/2} / \Xi_{2n-1},$$

$$V_{2n+1}^- = d_{2n+1}^{+*} e^{(\gamma_{2n+1} + \gamma_{2n+2})/2} / \Xi_{2n+2},$$

$$V_{2n-1}^+ = -\sigma_{2n} \sigma_{2n-1} d_{2n-1}^{-*} e^{-(\gamma_{2n} + \gamma_{2n-1})/2} / \Xi_{2n},$$

where the quantities  $\Xi_n$  are defined as

$$\Xi_{2n} = r_{2n}^{+*} e^{\gamma_{2n}} - r_{2n}^{-*} e^{-\gamma_{2n}},$$

$$\Xi_{2n-1} = r_{2n-1}^{+*} e^{\gamma_{2n-1}} - r_{2n-1}^{-*} e^{-\gamma_{2n-1}}. \quad (\text{A2})$$

In nonresonant junctions, the functions  $\Xi_n$  approach  $r\xi_n$  since energy dispersion of the reflection amplitude is negligibly small. SGS in nonresonant junctions is caused by zeros of the functions  $\xi_n$ ,<sup>4</sup> and renormalization of these functions in the resonance case,  $\xi_n \rightarrow \Xi_n$ , is the reason for the considerable difference between the SGS in resonant and nonresonant junctions. We solve Eqs. (A1) by introducing ratios  $S_{2n} = c_{2n}/f_{2n-1}$  and  $S_{2n+1} = f_{2n+1}/c_{2n}$  and expressing  $f_n$  through  $c_0$ ,

$$f_n = \prod_{i=0}^n S_i c_0, \quad (\text{A3})$$

$c_0$  being related to  $S_{\pm 1}$  by virtue of the first equation in Eq. (A1). By introducing chain fractions  $Z_n$ ,

$$Z_0 = 1 - (d_0^{+*})^2 \frac{e^{\gamma_0}}{\Xi_0 \Xi_1 Z_1} - (d_0^{-*})^2 \frac{e^{-\gamma_0}}{\Xi_0 \Xi_{-1} Z_{-1}}, \quad (\text{A4})$$

$$Z_{2n} = 1 - (d_{2n}^{+*})^2 \frac{e^{-\gamma_{2n} - \gamma_{2n-1}}}{\Xi_{2n} \Xi_{2n-1} Z_{2n-1}},$$

$$Z_{2n-1} = 1 - (d_{2n-1}^{+*})^2 \frac{e^{\gamma_{2n-1} + \gamma_{2n-2}}}{\Xi_{2n-1} \Xi_{2n-2} Z_{2n-2}},$$

one can rewrite Eq. (A3) for  $f_n$ , e.g., with negative sideband index  $n = -2k - 1 < 0$ , in the following form:

$$f_{-2k-1} = \frac{2\xi}{\Delta} (-1)^k d_0^{-*} e^{-(\gamma + \gamma_{-2k-1})/2} \times \prod_0^{2k+1} \frac{\sigma_{-i}}{\Xi_{-i} Z_{-i}} \prod_1^k d_{-2i}^{+*} d_{-2i}^{-*}. \quad (\text{A5})$$

An equation for  $b_{-2k-1}$  follows from Eqs. (11) and (A5),

$$b_{-2k-1} = r_{-2k-2}^{+*} e^{\gamma_{-2k-1}} \times \left( 1 + \frac{D_{-2k-2}^+ e^{\gamma_{-2k-2}}}{r_{-2k-2}^+ \Xi_{-2k-2} Z_{-2k-2}} \right) f_{-2k-1}, \quad (\text{A6})$$

where  $D_n^\pm = |d_n^\pm|^2$ .

Collecting the normal and Andreev transmission amplitudes in Eqs. (A5) and (A6) and substituting them into Eq. (15) for the current, we finally get

$$K_n = -|f_n|^2 \cosh(\text{Re } \gamma_n) \left( 1 - e^{2 \text{Re } \gamma_n} (1 - D_{n-1}^+) \times \left| 1 + \frac{D_{n-1}^+ e^{\gamma_{n-1}}}{r_{n-1}^+ \Xi_{n-1} Z_{n-1}} \right|^2 \right) \quad n < 0. \quad (\text{A7})$$

The corresponding equation for positive  $n > 0$  is obtained from Eq. (A7) via the substitutions  $\gamma \rightarrow -\gamma$ ,  $D^+ \rightarrow D^-$ , and  $n-1 \rightarrow n+1$ .

### APPENDIX B: TRANSFORMATION OF $K_n$

Equation (A7) is not convenient for analysis of the subharmonic gap structure.<sup>4</sup> The current structures are caused by the processes of creation of real excitations during across-the-gap transitions  $E \rightarrow E_n < -\Delta$ . The currents of other sidebands ( $E_n > \Delta$ ) perfectly cancel each other at zero temperature.<sup>7</sup> Furthermore, there is rigorous balance between Andreev and normal channel currents among the states lying within the superconducting gap,<sup>7</sup> which provides successive drops of the current with decreasing applied voltage. All of these features are not explicitly seen in the currents  $K_n$  in Eq. (A7). Moreover, the current structures related to the creation of real excitations in even-order sidebands are hidden in Eq. (17) which consists of contributions from only odd sidebands.

To overcome this difficulty, we will transform the side-

band currents in Eq. (A7) following the method suggested in Ref. 4. Assuming the transparency  $D_{n-1}^+$  in Eq. (A7) to be small, we find that the current  $K_n$  to leading order is proportional to  $\sinh(\text{Re } \gamma_n) \sim \theta(E_n^2 - \Delta^2)$ . This observation allows us [in Eq. (19)] to separate the contributions from states below,  $E_n < -\Delta$ , and above,  $E_n > -\Delta$  the energy gap. Having separated out the leading term, we rewrite Eq. (A7) in the form

$$K_n = |f_n|^2 \cosh(\text{Re } \gamma_n) \left( 2 \sinh(\text{Re } \gamma_n) e^{\text{Re } \gamma_n} - \frac{D_{n-1}^+ e^{2 \text{Re } \gamma_n}}{|\Xi_{n-1} Z_{n-1}|^2} F_{n-1} \right), \quad (\text{B1})$$

$$F_n = |\Xi_n Z_n|^2 - 2 \text{Re}(e^{\gamma_n} r_n^+ \Xi_n Z_n) - D_n^+ e^{2 \text{Re } \gamma_n}. \quad (\text{B2})$$

Equation (B2) possesses a similar property: it is proportional to  $\theta(E_n^2 - \Delta^2)$  to leading order with respect to  $D$ . Separating out this leading term, we further transform Eq. (B2) into the equation

$$F_n = -2 \sinh(2 \text{Re } \gamma_n) - \frac{D_n^- e^{-2 \text{Re } \gamma_n}}{|\Xi_{n-1} Z_{n-1}|^2} G_{n-1}, \quad (\text{B3})$$

where

$$G_{n-1} = |\Xi_{n-1} Z_{n-1}|^2 + 2 \text{Re}(e^{-\gamma_{n-1}} r_n^- \Xi_{n-1} Z_{n-1}) - D_n^- e^{-2 \text{Re } \gamma_{n-1}}. \quad (\text{B4})$$

One more transformation,

$$G_{n-1} = 2 \sinh(2 \text{Re } \gamma_{n-1}) - \frac{D_{n-2}^+ e^{2 \text{Re } \gamma_{n-1}}}{|\Xi_{n-2} Z_{n-2}|^2} F_{n-2}, \quad (\text{B5})$$

accomplishes the cycle, yielding the quantity  $F$  in Eq. (B2) with shifted index. Performing repeatedly such transformations, we get for the current in Eq. (A7) the following expansion:

$$\begin{aligned} K_n &= \theta(E_n^2 - \Delta^2) Q_n + 2 \theta(E_{n-1}^2 - \Delta^2) \\ &\times e^{-\text{Re } \gamma_n} \cosh(\text{Re } \gamma_n) Q_{n-1} + 2 \theta(E_{n-2}^2 - \Delta^2) \\ &\times e^{-\text{Re } \gamma_n + 2 \text{Re } \gamma_{n-1}} \cosh(\text{Re } \gamma_n) Q_{n-2} + 2 \theta(E_{n-3}^2 - \Delta^2) \end{aligned}$$

$$e^{-\text{Re } \gamma_n + 2 \text{Re } \gamma_{n-1} - 2 \text{Re } \gamma_{n-2}} \cosh(\text{Re } \gamma_n) Q_{n-3} + \dots \quad (\text{B6})$$

In this equation, the quantity  $Q_n$  is defined as

$$Q_n = \frac{8 \xi^2 \xi_n |E_n| e^{-\gamma}}{\Delta^4 P_n} D_0^- \left( \prod_{i=1}^{k-1} D_{-2i}^+ D_{-2i}^- \right) \times D_{-2k}^+ \begin{cases} 1, & |n| = 2k \\ D_{-2k}^-, & |n| = 2k + 1, \end{cases} \quad (\text{B7})$$

where

$$P_n = \prod_{i=0}^{|n|} |\Xi_{-i} Z_{-i}|^2. \quad (\text{B8})$$

Collecting together all terms with similar  $\theta$  functions, we can finally rearrange the sum in Eq. (18):

$$\sum_{n=\text{odd}} K_n \rightarrow \sum_{n=1}^{\infty} \tilde{K}_n, \quad \tilde{K}_n = \theta(E_n^2 - \Delta^2) Q_n \varphi_n, \quad (\text{B9})$$

where  $\varphi_n$  is given by the recurrence equation

$$\varphi_{n-1} = 1 + \exp[(-1)^{n+1} 2 \text{Re}(\gamma_n)] \varphi_n, \quad \varphi_{-1} = 1.$$

Far from resonance, the quantity  $P_n$  may cause strong singularity in the sideband current due to the presence of zeros in the functions  $\Xi_n$ , and accounting for the factors  $Z_n$  is absolutely necessary for regularization of the singularity.<sup>4</sup> In the resonant case, the functions  $\Xi_n$  do not tend to zero because of strong electron-hole dephasing,  $r_n^+ \neq r_n^-$ , and the quantities  $Z_n$  can be omitted from Eq. (B8) in the limit of narrow resonance  $\Gamma \ll \Delta$ ,

$$P_n \approx \prod_{i=0}^n |\Xi_{-i}|^2. \quad (\text{B10})$$

The role of  $Z_n$  in this limit reduces to cancellation of the terms in the product (B10) which are proportional to the squared resonance amplitudes  $(d_n^\pm)^2$ ; this is denoted by the prime in Eq. (B10). The presence of the resonant denominators in Eq. (A2) for  $\Xi$  gives rise to renormalization of the normal electron transmission coefficients  $D_n^\pm$  in Eq. (19) for the current.

<sup>1</sup>N. van der Post, E.T. Peters, I.K. Yanson, and J.M. van Ruitenbeek, Phys. Rev. Lett. **73**, 2611 (1994).

<sup>2</sup>E. Scheer, P. Joyez, M.H. Devoret, D. Esteve, and C. Urbina, Phys. Rev. Lett. **78**, 3535 (1997).

<sup>3</sup>E.N. Bratus', V.S. Shumeiko, and G. Wendin, Phys. Rev. Lett. **74**, 2110 (1995).

<sup>4</sup>V.S. Shumeiko, E.N. Bratus', and G. Wendin, Low Temp. Phys. **23**, 181 (1997).

<sup>5</sup>D. Averin and A. Bardas, Phys. Rev. Lett. **75**, 1831 (1995).

<sup>6</sup>J.C. Cuevas, A. Martin-Rodero, and A. Levy Yeyati, Phys. Rev. B **54**, 7366 (1996).

<sup>7</sup>E.N. Bratus', V.S. Shumeiko, E.V. Bezuglyi, and G. Wendin, Phys. Rev. B **55**, 12 666 (1997).

<sup>8</sup>E. Scheer *et al.*, Nature (London) **394**, 154 (1998).

<sup>9</sup>S.J. Tans *et al.*, Nature (London) **386**, 474 (1997).

<sup>10</sup>M. Bockrath *et al.*, Science **275**, 1922 (1997).

<sup>11</sup>D.C. Ralph, C.T. Black, and M. Tinkham, Phys. Rev. Lett. **74**, 3241 (1995).

<sup>12</sup>A. Yacobi, M. Heiblum, D. Mahalu, and H. Shtrikman, Phys. Rev. Lett. **74**, 4047 (1995).

<sup>13</sup>L.G. Aslamazov and V.M. Fistul, Zh. Éksp. Teor. Fiz. **81**, 382 (1981) [Sov. Phys. JETP **54**, 206 (1981)].

- <sup>14</sup>A.T. Tartakovsky and V.M. Fistul', Zh. Éksp. Teor. Fiz. **94**, 353 (1988) [Sov. Phys. JETP **67**, 1935 (1988)].
- <sup>15</sup>I.F. Itskovich and R.I. Shekhter, Fiz. Nizk. Temp. **7**, 863 (1981) [Sov. J. Low Temp. Phys. **7**, 418 (1981)].
- <sup>16</sup>L.A. Devyatov and M. Yu. Kupriyanov, Pis'ma Zh. Éksp. Teor. Fiz. **59**, 187 (1984) [JETP Lett. **59**, 200 (1994)].
- <sup>17</sup>P.I. Arseyev and B.A. Volkov, Solid State Commun. **78**, 373 (1991).
- <sup>18</sup>C.W.J. Beenakker and H. van Houten, *Single Electron Tunneling and Mesoscopic Devices* (Springer, Berlin, 1991).
- <sup>19</sup>G. Wendin and V.S. Shumeiko, Superlattices Microstruct. **20**, 569 (1996).
- <sup>20</sup>G. Johansson, E. Bratus', V.S. Shumeiko, and G. Wendin, Physica C **293**, 77 (1997).
- <sup>21</sup>A. Levy Yeyati, J.C. Cuevas, A. Lopez-Davalos, and A. Martin-Rodero, Phys. Rev. B **55**, R6137 (1997).
- <sup>22</sup>I.L. Aleiner, Penny Clarke, and L.I. Glazman, Phys. Rev. B **53**, R7630 (1996).
- <sup>23</sup>A. Golub, Phys. Rev. B **52**, 7458 (1995).
- <sup>24</sup>L.I. Glazman and K.A. Matveev, Pis'ma Zh. Éksp. Teor. Fiz. **49**, 570 (1989) [JETP Lett. **49**, 659 (1989)].
- <sup>25</sup>R. Landauer, IBM J. Res. Dev. **1**, 223 (1957).
- <sup>26</sup>M.A. Büttiker, Phys. Rev. Lett. **57**, 1761 (1986).
- <sup>27</sup>Y. Imry, *Directions in Condensed Matter Physics* (World Scientific, Singapore, 1986) p. 102.
- <sup>28</sup>Note that the normal double barrier region is treated exactly, not in the quasiclassical approximation.
- <sup>29</sup>A definition of long SIS junctions was introduced in G. Wendin and V.S. Shumeiko, Phys. Rev. B **53**, R6006 (1996).
- <sup>30</sup>T.M. Klapwijk, G.E. Blonder, and M. Tinkham, Physica B & C **109-110**, 1657 (1982).
- <sup>31</sup>S.J. Tans, Ph.D. thesis, Delft University, 1998.
- <sup>32</sup>Yu. V. Nazarov, Physica B **189**, 57 (1993).
- <sup>33</sup>N.C. van der Vaart *et al.*, Phys. Rev. Lett. **74**, 4702 (1995).
- <sup>34</sup>H. Takayanagi, T. Akazaki, and J. Nitta, Phys. Rev. Lett. **75**, 3533 (1995).
- <sup>35</sup>R. Kleiner and P. Müller, Phys. Rev. B **49**, 1327 (1994).